Supporting information

A New and high Li^+ conductive Mg doped $Li_{1.5}Al_{0.5}Ge_{1.5}(PO_4)_3$ Solid Electrolyte with Enhanced Electrochemical Performance for Solid-State Lithium Metal Battery

Yosef Nikodimos[a,c], Ljalem Hadush Abrha[a], Haile Hisho Weldeyohannes[a], Kassie Nigus Shitaw[a], Nigusu Tiruneh Temesgen [a], Bizualem Wakuma Olbasa[a], Chen-Jui Huang [a], Shi-Kai Jiang [a], Chia-Hsin Wang[e], Hwo-Shuenn Sheu[e], She-Huang Wu[b, c, f,*], Wei-Nien Su[b,f,*], Chun-Chen Yang[c,d, *], Bing Joe Hwang[a, e, f, *]

a. Nano-electrochemistry Laboratory, Department of Chemical Engineering, National Taiwan University of Science and Technology, Taipei city 106, Taiwan

b. Nano-electrochemistry Laboratory, Graduate Institute of Applied Science and Technology, National Taiwan University of Science and Technology, Taipei city 106, Taiwan

c. Battery Research Center of Green Energy, Ming Chi University of Technology, New Taipei City 24301, Taiwan

d. Department of Chemical Engineering, Ming Chi University of Technology, New Taipei City 24301, Taiwan

e. National Synchrotron Radiation Research Center (NSRRC), Hsinchu 30076, Taiwan

f. Sustainable Energy Development Center, National Taiwan University of Science and Technology, Taipei city 106, Taiwan

Transference number calculation: To further examine the influence of Mg as dopant on LAGP electrolyte, the transference number was estimated computationally from AIMD simulations. The mobility of each atom was investigated from their respective mean square displacement (MSD) profile. The diffusion value has been determined from the slope of MSD plots for each ion in the LAMGP material from the MSD slope. The transference number of the LAMGP material was determined from the D ratio as follow[1]:

$$t_{Li^+} = \frac{D_{Li^+}}{D_{Li^+} + D_{Al^{3+}} + D_{Mg^{2+}} + D_{Ge^{4+}} + D_{P^{5+}} + D_{O^{2-}}} \quad (5)$$

Results

From the diffusion (D) values in the temperature range of 600-1400 ^oC, the diffusion value at 25 ^oC was determine by extrapolation followed by ionic conductivity(σ_{Li}^+) calculation using Equation (3). The values of D, σ and E_a for each composition are summarized in Table S1.

Table S1: Summery for the computational analysis of ionic conductivity at room temperature for the prepared samples

$Li_{1+x+2y}Al_xMg_yGe_{2-x-y}(PO_4)_3$	$D \times 10^{-6}$ (cm^2/s)	σ ($mS\ cm^{-1}$)	E_a (eV)
LAGP	0.821±0.003	3.626	0.286
LAMGP	2.55±0.005	7.996	0.261
LAMGP2	1.19±0.008	4.602	0.280
LAMGP3	0.0285±0.005	0.550	0.336
LAMGP4	0.0179±0.009	0.232	0.358
LMGP	0.0869±0.007	0.102	0.405

The Li^+ MSD profile shown in Figure S1 indicates a linear increase with the time step, showing that Li^+ mobility among different sites and transport over the lattice. In contrast, the MSD profile for the other ions (Al, Mg, Ge P and O) is constant shows they remained close to their original position during the AIMD run. The noted zero slope from their MSD profiles essentially show they vibrate only about their original sites. Similar result was obtained at all simulation temperatures between 700 K and 1400 K.

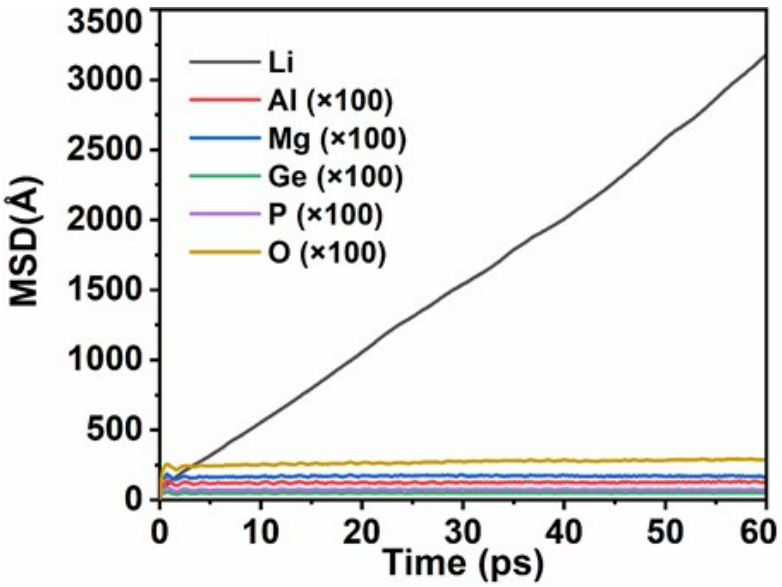

Figure S1: MSD plots of Li, Al, Mg, Ge, P, and O ions in $Li_{1.6}Al_{0.4}Mg_{0.1}Ge_{1.5}(PO_4)_3$ at 600 K. Plots for Al, Mg, Ge, P, and O are magnified by a factor of 100 to illustrate their behaviors.

As can be seen from Figure S2 of XRD patterns, the NASICON type structure of LAGP crystal was formed at all crystallization temperatures. At higher crystallization (850 ^{o}C), impurities like GeO_2 and $AlPO_4$ were observed.

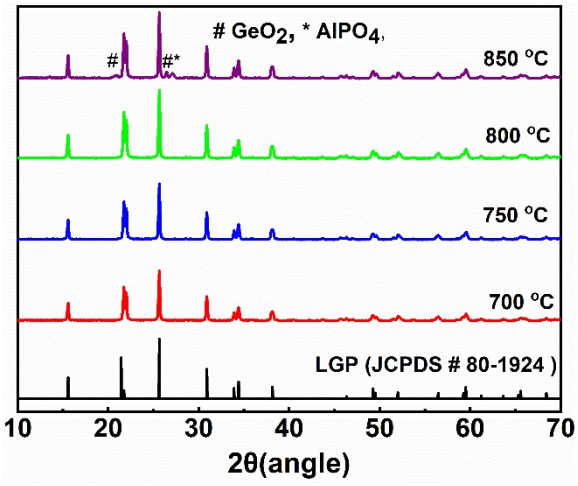

Figure S2: XRD patterns of LAGP specimen crystalized at different crystallization temperatures.

The SXRD pattern Rietveld refinement analysis for the samples crystalized at 700, 750, 800 and 850 ^{o}C are presented in Figure S3, while the structural parameters from the refinement are summarized in Table S2 and S3. From the Rietveld refinement results of all samples, the formation of a NASICON type dominant rhombohedral LGP structure with $R\bar{3}c$ space group was confirmed. For the LAMGP sample crystalized at 750 ^{o}C, the lattice parameters were obtained equal to a = 8.281 Å and c = 20.680 Å, in an excellent agreement with a = 8.25 Å and c = 20.46 Å (JCPDS 80−1924). These observations indicated the formation a NASICON-type LAMGP crystalline phase even though Ge^{4+} is partly replaced by Al^{3+} and Mg^{2+}. The slight increment of LAMGP lattice parameters due to larger ionic radius of Mg^{2+} ion led to insignificant structural alteration. With increasing crystallization temperature, the lattice parameters have been decreased which is due to the formation of impurities at higher

temperature. Therefore, the higher the impurity at higher crystallization temperature, the smaller LAMGP lattice parameters were obtained.

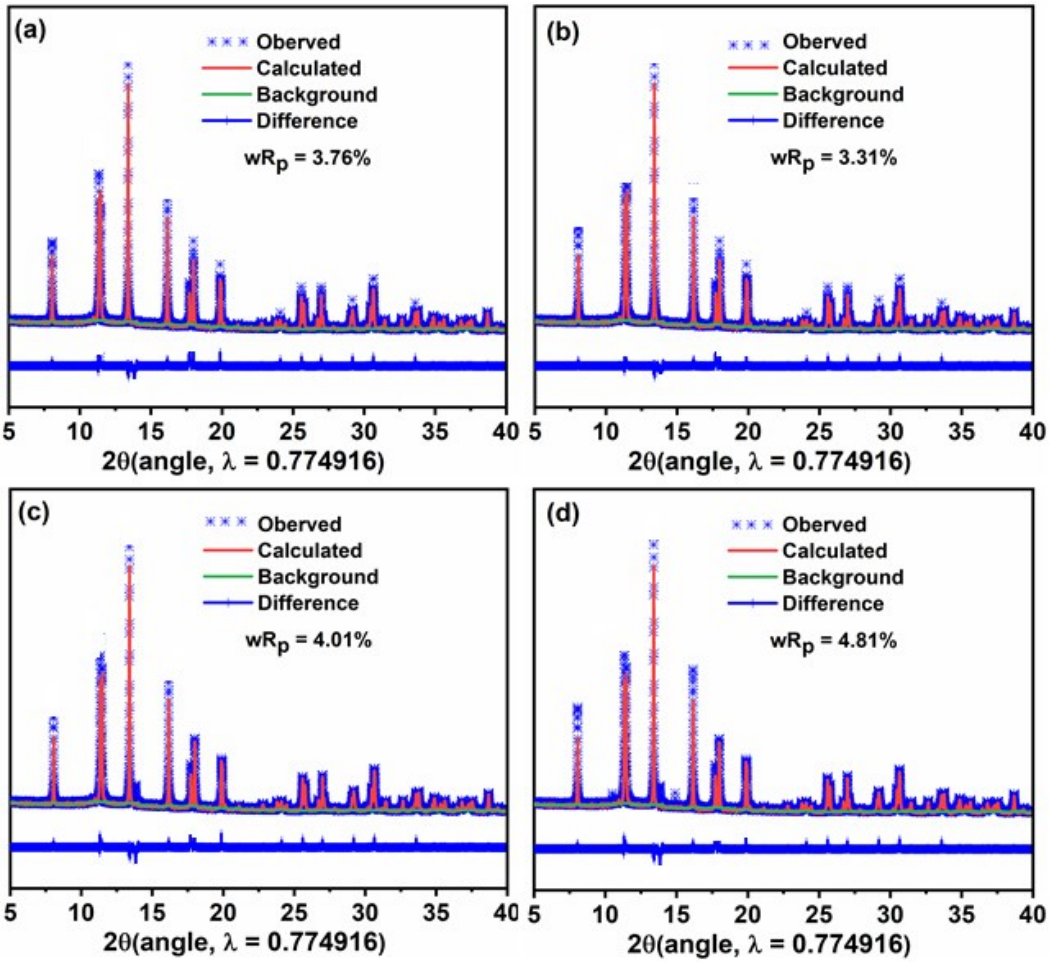

Figure S3: SXRD Rietveld refinement of LAMGP samples with a space group of $R\bar{3}c$ and crystallization temperature of (a) 700 °C (b) 750 °C (c) 800 °C and (d) 850 °C.

Lattice parameters of LAGP and LAMGP samples comparison were retrieved from the Rietveld refinement analysis, as shown in Table S3, in order to understand the effect of Mg^{2+} on the materials dimension. Even though they are synthesized in the same procedure, the lattice parameters of LAMGP are larger than that of LAGP, which is as a result of Mg^{2+}'s larger ionic radius which is an advantage to enhance the ionic conductivity.

Table S2: Structural parameters of LAMGP (space group of R-3c) from the Rietveld refinement

Atom	Position	Occupancy	Wyckoff site
Li1(M1)	0.0, 0.0, 0.0	0.801	6b
Li2(M2)	0.0, 0.25, 0.05	0.146	36f
Ge	0.0, 0.0, 0.141	0.752(3)	12c
Al	0.0, 0.0, 0.141	0.1984(3)	12c
Mg	0.0, 0.0, 0.141	0.0496(3)	12c
P	0.288, 0.000, 0.250	1	18e
O1	0.180, -0.015, 0.188	1	36f
O2	0.185, 0.159, 0.082	1	36f

Table S3: Lattice parameters of LAGP and LAMGP electrolytes at different crystallization temperatures.

Crystallization temperature		a(Å)	c(Å)	V(Å^3)	R_p	wR_p
700 °C	**LAGP**	8.250	20.475	1220. 550	4.93%	4.29%
	LAMGP	8.276	20.667	1223.003	4.06%	3.76%
750 °C	**LAGP**	8.253	20.477	1220.555	4.52%	4.43%
	LAMGP	8.281	20.680	1223.976	3.31%	3.31%
800 °C	**LAGP**	8.254	20.478	1220.602	3.68%	3.96%
	LAMGP	8.274	20.619	1222.103	3.73%	4.01%
850 °C	**LAGP**	8.249	20.391	1219.215	4.32%	4.69%
	LAMGP	8.269	20.470	1220.459	4.97%	4.81%

Table S4: Composition analysis of elements in LAMGP ($Li_{1.6}Al_{0.4}Mg_{0.1}Ge_{1.5}(PO_4)_3$) samples from ICP-OES measurements

Crystallization Temperature	Weight %					Chemical formula
	Li	Al	Mg	Ge	P	
700 °C	4.912	4.780	1.085	48.144	41.079	$Li_{1.602}Al_{0.401}Mg_{0.101}Ge_{1.5}P_{3.002}O_{12}$
750 °C	4.910	4.782	1.074	48.157	41.077	$Li_{1.601}Al_{0.401}Mg_{0.1}Ge_{1.5}P_{3.001}O_{12}$
800 °C	4.907	4.743	1.055	48.212	41.083	$Li_{1.597}Al_{0.397}Mg_{0.098}Ge_{1.499}P_{2.996}O_{12}$
850 °C	4.891	4.727	1.056	48.229	41.097	$Li_{1.589}Al_{0.395}Mg_{0.098}Ge_{1.497}P_{2.992}O_{12}$

Figure S4 shows EDX elemental analysis of the LAMGP samples crystalized at different temperatures. The analysis was conducted on grains surface (shaped crystals) and specified points of grain boundaries. Results of the analysis are summarized in Table S5 and S6.

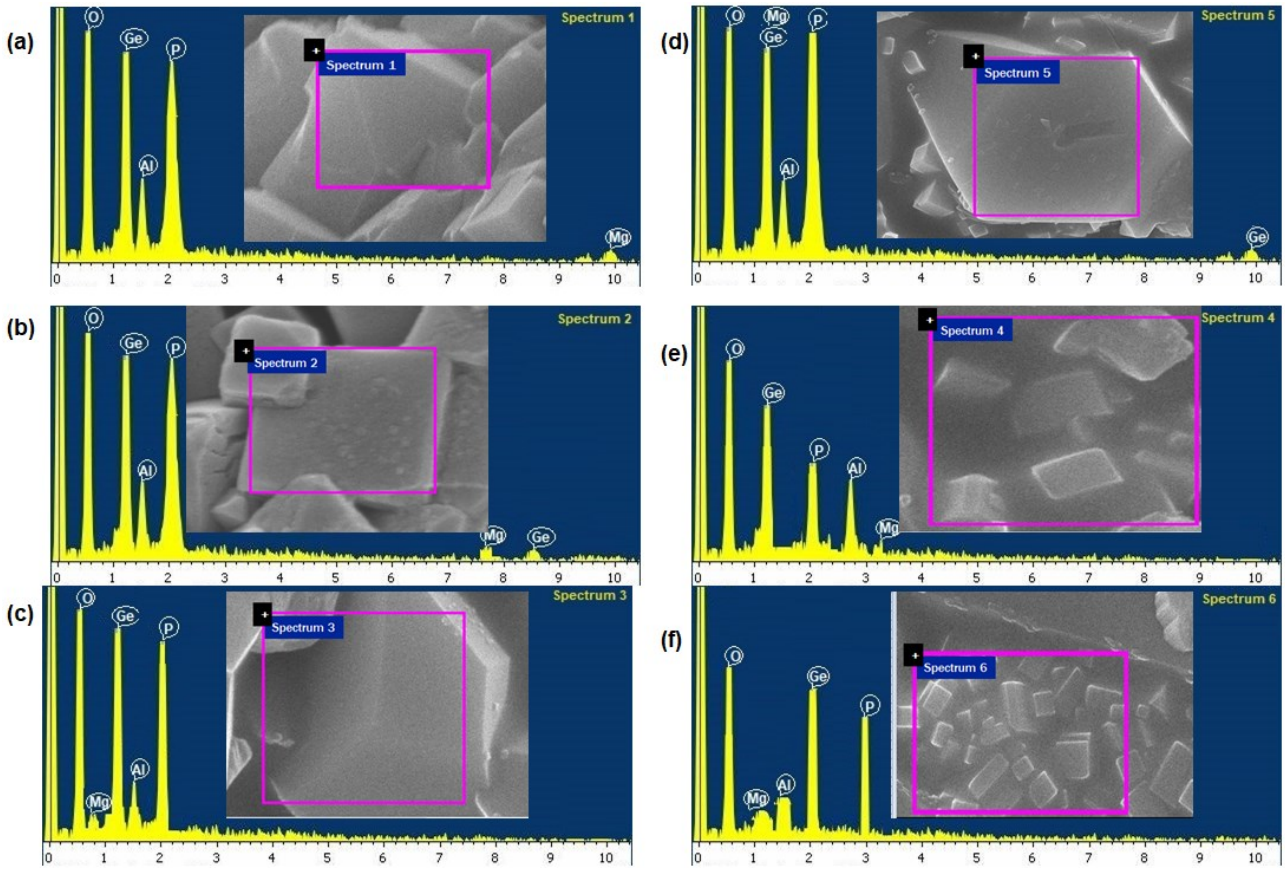

Figure S4: EDX analysis of LAMGP at intragrain (a). 700 ^{o}C, (b). 750 ^{o}C, (c). 800 ^{o}C, (d). 850 ^{o}C and grain boundary (e). 800 ^{o}C, (f). 850 ^{o}C.

Table S5 shows the stoichiometric composition at grains of the LAMGP samples which were crystalized at different temperatures.

Table S5: EDX analysis of LAMGP at intragrain crystalized at different temperatures

Element	EDX analysis (weight%)			
	700 °C	750 °C	800 °C	850 °C
Al	2.651	2.655	2.485	2.208
Mg	0.597	0.598	0.599	0.497
Ge	26.727	26.684	26.402	26.197
P	22.896	22.852	22.745	22.021
O	47.129	47.211	47.769	49.077
Li	-	-	-	-
Overall formula	$Li_{1.6}Al_{0.4}Mg_{0.1}Ge_{1.498}P_{3.01}O_{12}$	$Li_{1.6}Al_{0.4}Mg_{0.1}Ge_{1.493}P_{2.999}O_{12}$	$Li_{1.6}Al_{0.37}Mg_{0.099}Ge_{1.46}P_{2.95}O_{12}$	$Li_{1.6}Al_{0.32}Mg_{0.08}Ge_{1.498}P_{2.78}O_{12}$

Table S6 shows the stoichiometric composition of the impurities at grain boundaries for the LAMGP samples which were crystalized at 800 °C and 850 °C.

Table S6: EDX analysis (in wt%) of LAMGP at the grain boundaries crystalized at different temperatures

Element	**800 °C**	**850 °C**
Al	11.847	5.256
Mg	0.534	4.736
Ge	31.895	28.301
P	13.598	18.099
O	42.126	43.608
Result	$GeO_2 + AlPO_4$	$GeO_2 + AlPO_4 + MgGe(PO_4)_2$

Figure S5 shows the grain size difference between LAGP and LAMGP. There was a significant grain size enhancement after LAGP doped by Mg^{2+}.

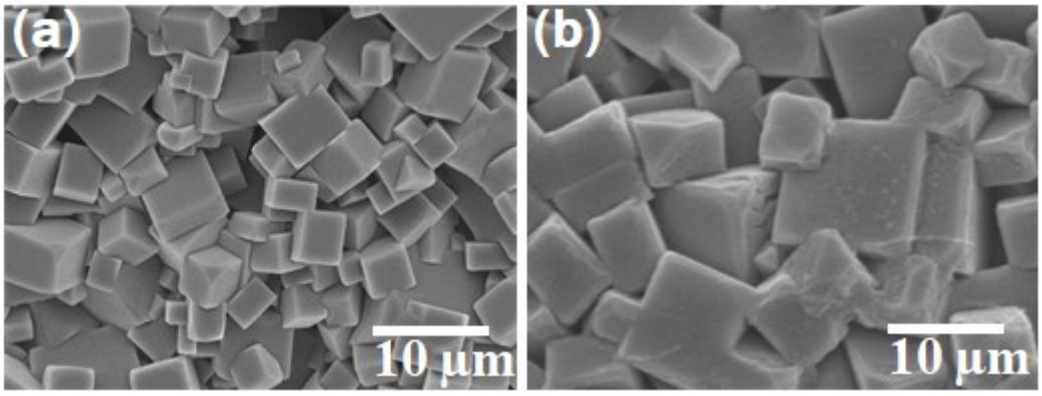

Figure S5: Grain size comparison of (a) LAGP and (b) LAMGP

Before gold sputtering, atomic force microscopy (AFM) images were measured (Figure S6) to check the roughness of the LAMGP pellets crystalized at different temperatures. Even though, the grain size is at µm level, the roughness was *ca.* 4.01, 4.69, 6.03 and 7.87 nm for 700-850 ^{o}C crystallization temperatures, respectively, which show the smoothness of the pellets.

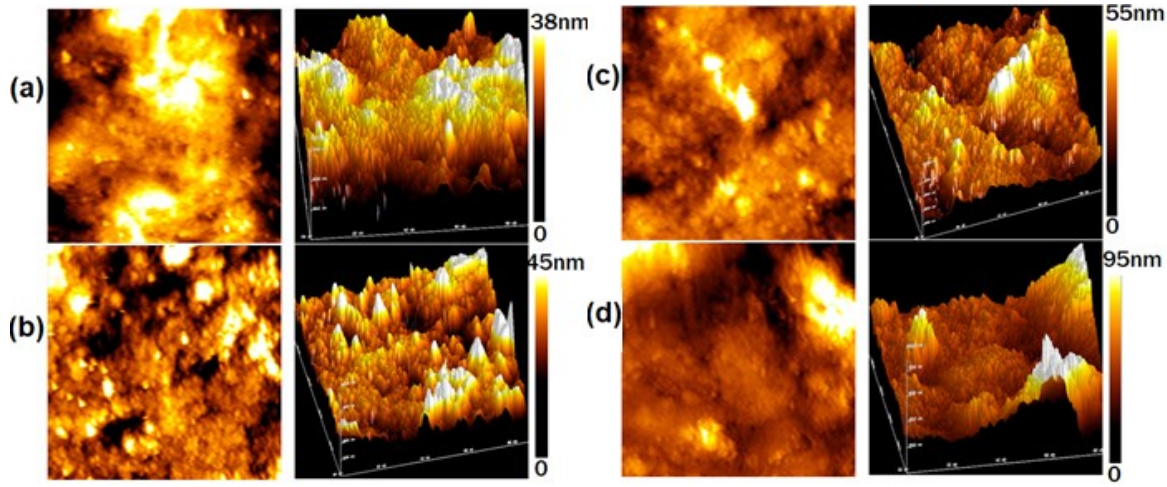

Figure S6: AFM topography images of LAMGP pellets obtained from different crystalized temperatures (a). 700 ^{o}C, (b). 750 ^{o}C, (c). 800 ^{o}C and (d). 850 ^{o}C, measured with a scan size of 15.7 µm × 17.9 µm. Right: 2D and left: 3D

EIS Nyquist plots were recorded for LAGP samples crystalized in the temperature range of between 700 – 850 ^{o}C. As can be seen from Figure S7, the highest ionic conductivity and lowest activation energy for LAGP was obtained at 800 ^{o}C crystallization temperature.

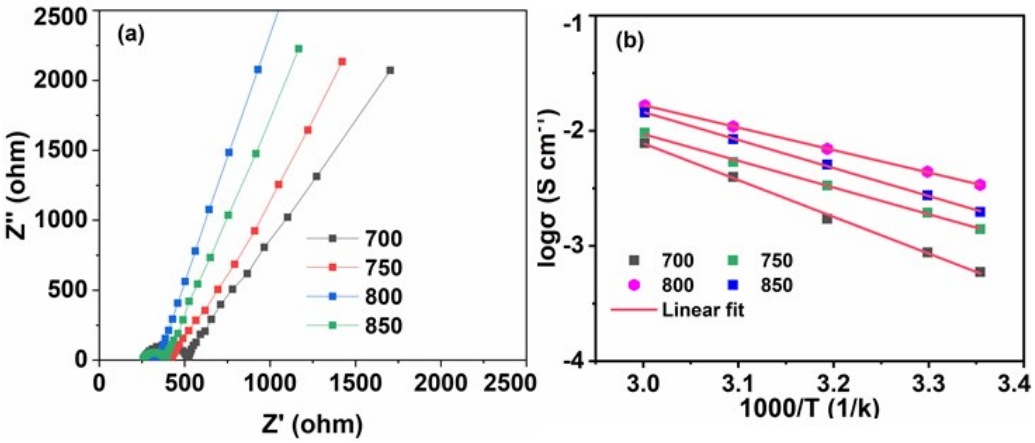

Figure S7: (a) Nyquist plot of LAGP electrolyte crystalized at various temperatures measured at 25 ^{o}C, (b). ionic conductivities of LAGP electrolytes varied with temperatures

Table S7 summarizes the bulk, grain boundary and total ionic conductivities of LAGP and LAMGP samples crystalized at different temperatures. Furthermore, grain size and relative densities of these samples are displayed. As shown in Table S7, when crystallization temperature increase grain size was also increased. However, relative density was decreased at higher crystallization temperature due to the formation of impurities. Overall, LAMGP sample crystalized at 750 ^{o}C is the best in all aspects relative to the remaining samples.

Table S7: Conductivities, E_a and relative densities of LAMGP and LAGP pellets at various crystallization temperatures.

Crystallization Temperature		**σ(mS cm^{-1})**			**E_a**	**Relative density**	Grain size (μm)
		σ_b	**σ_{gb}**	**σ_T**			
700	LAGP	0.507	0.081	0.118	0.50±0.02	88.4%	1.097
	LAMGP	0.863	0.218	0.371	0.31±0.03	90.2%	9.946
750	LAGP	0.997	0.233	0.396	0.35±0.03	90.5%	1.847
	LAMGP	7.435	1.51	0.913	0.28±0.01	96.3%	12.059
800	LAGP	2.896	0.642	0.516	0.29±0.02	93.8%	3.573
	LAMGP	4.84	0.830	0.417	0.28±0.02	94.3%	13.817
850	LAGP	1.514	0.351	0.428	0.32±0.03	92.7%	5.182
	LAMGP	3.68	0.427	0.259	0.29±0.04	92.9%	15.089

As can be seen from Table S8, the Mg doped LAGP electrolyte offered the highest Li^+ conductivity (bulk, grain boundary and total) relative to previously reported LAGP based electrolytes synthesized using the same approach, a melt-quenching method.

Table S8: Comparison of ionic conductivities at room-temperature for LAGP based solid electrolytes synthesized using a melt-quenching method.

Sample	Crystall. temperature (^oC)	σ (mS cm^{-1})			E_a (eV)	Ref.
		bulk	gb	total		
$Li_{1.5}Al_{0.5}Ge_{1.5}(PO_4)_3$	825	4.22			0.3	2
$Li_{1.5}Al_{0.4}Cr_{0.1}Ge_{1.5}(PO_4)_3$	850	6.65			0.292	3
$Li_{1.5}Al_{0.33}Sc_{0.17}Ge_{1.5}(PO_4)_3$	800	5.826			0.282	4
$Li_{1.6}Al_{0.4}Ba_{0.1}Ge_{1.5}(PO_4)_3$	750	0.88	1	0.47	0.314	5
$Li_{1.5}Al_{0.5}Ge_{1.5}(PO_4)_3$–$0.05Li_2O$	800	1.18		0.725	0.31	6
$Li_{1.5}Al_{0.5}Ge_{1.5}(PO_4)_3$	850	5.08			0.373	7
$Li_{1.6}Al_{0.4}Mg_{0.1}Ge_{1.5}(PO_4)_3$	750	7.435	1.51	0.913	0.275	**This work**

Figure S9 (a) shows XRD patterns for LAMGP samples prepared from $Mg_3(PO_4)_2$, MgO and $MgCO_3$ precursors. Each of them displays a typical NASICON type structure similar to LGP (JCPDS # 80-1924 index file). However, visible impurities were detected for the MgO and $MgCO_3$ precursors. The appearance of MgO in the XRD patterns is an indication there is still unmolten MgO in the material due to its very high melting point (ca. 2852 ^{o}C). Figure S9 (b) shows the Nyquist plots recorded at 25 ^{o}C for LAMGP samples synthesized from the possible different types of Mg precursors. All the plots show a semicircle at high-medium frequencies, which is connected with a diffusion tail at low frequencies. The total resistance (R_{total}) is associated with the semicircle, which is the sum of R_b and R_{gb}.

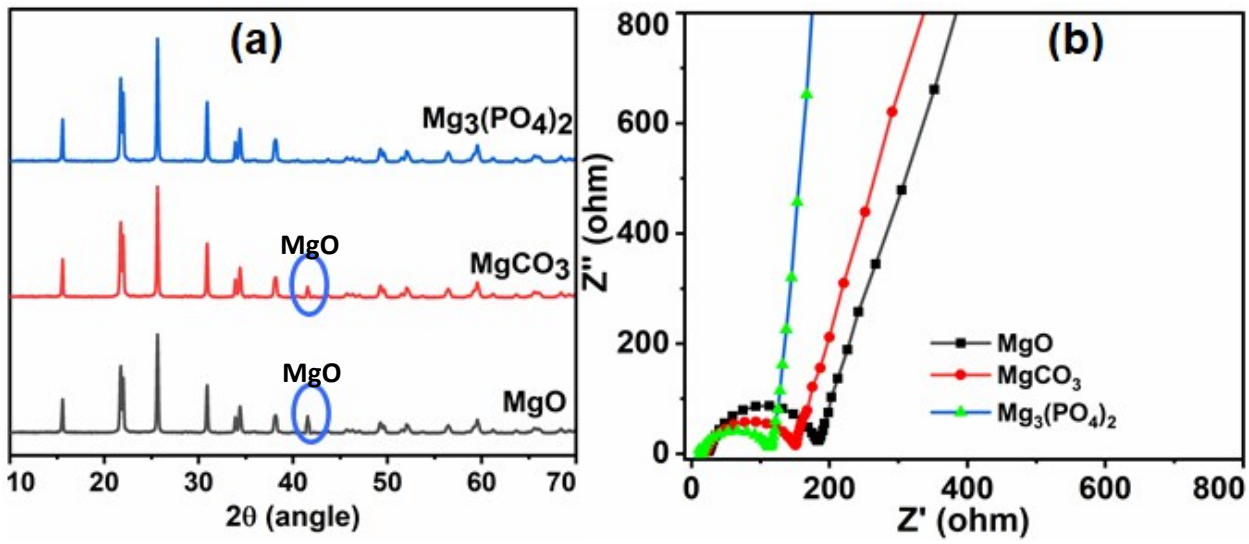

Figure S8: LAMGP electrolyte using different Mg precursors (a). XRD patterns (b). EIS Nyquist plots recorded at 25 ^{o}C

As shown in Figure S9, LAGP pellet is more porous relative to LAMGP pellet, indicating the densification of LAGP by doping using Mg^{2+}.

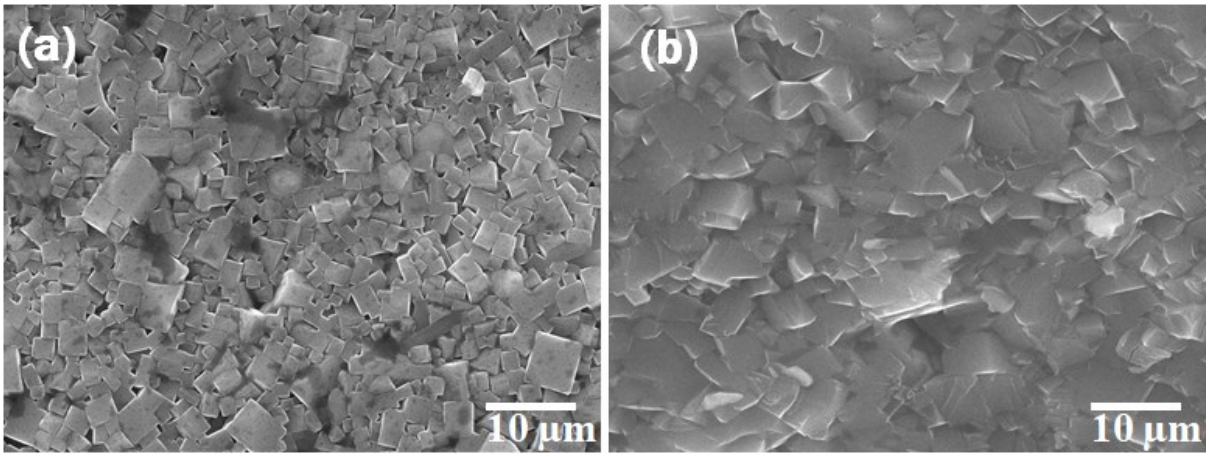

Figure S9: Cross-section SEM images (a) LAGP and (b) LAMGP pellets

Table S9 shows ionic conductivities, grain size and grain size of LAMGP samples synthesized from different Mg precursors. The LAMGP electrolyte which synthesized using $Mg_3(PO_4)_2$ as Mg precursor showed better properties in all aspects. The difference in grain boundary conductivity and densification among the samples is mainly due to the impurity at the grain boundaries and the samples' degree of porosity.

Table S9: Summary of Li^+ conductivity and relative density (RD) of LAMGP electrolyte prepared from different Mg precursors.

Crystallization temperature (^oC)	Precursor of Mg in LAMGP electrolyte								
	$Mg_3(PO_4)_2$			MgO			$MgCO_3$		
	σ (mS cm^{-1})		R.D (%)	σ (mS cm^{-1})		R.D (%)	σ (mS cm^{-1})		R.D (%)
	σ_b	σ_{gb}		σ_b	σ_{gb}		σ_b	σ_{gb}	
700	0.863	0.218	90.2	0.294	0.063	87.9	0.582	0.099	89.9
750	7.435	1.51	96.3	0.816	0.119	89.4	2.728	0.606	92.9
800	4.84	0.83	94.3	2.047	0.443	91.14	2.215	0.514	92
850	3.68	0.427	92.9	1.152	0.194	88.8	1.382	0.282	90.1

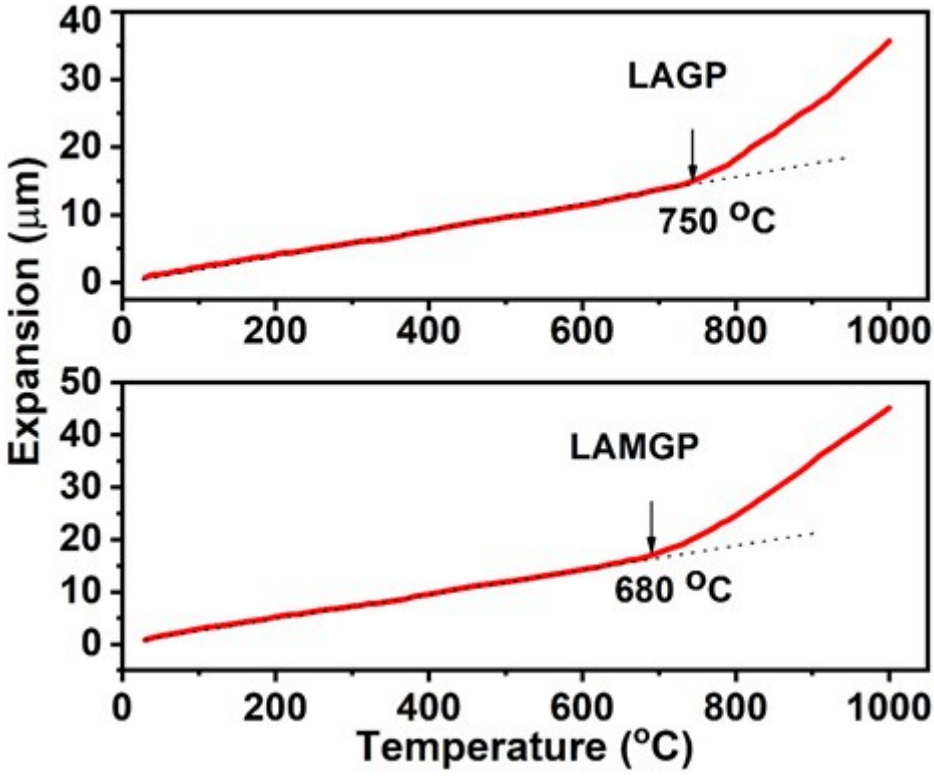

Figure S10: Thermomechanical analysis of LAGP and LAMGP pellets as a function of temperature.

Figure S11 shows photos of LAMGP pellets soaked in liquid electrolyte (LE) at the initial state and after 10 days. There was no any observable change in color of the pellet and the liquid electrolyte after 10 days, as shown in the photo.

Figure S11: Photos of LAMGP pellet in liquid electrolyte at the initial state and after 10 days.

SEM image and XRD pattern of the pellet were measured before and after soaking in the liquid electrolyte, then compared to each other to investigate if there is any significant difference between them. Figure S12 (a and b) presents SEM images of the LAMGP pellet before and after LE treatment. There was not a significant color and morphology change observed between the two cases, which have a dense ceramic surface and almost the same grain size of approximately 10-15 µm. Furthermore, as presented in Figure S12 (c and d), the XRD patterns for the LAMGP pellet before and after soaking in the liquid electrolyte well matched to each other, confirming that LAMGP is structurally stable in the mentioned liquid electrolyte.

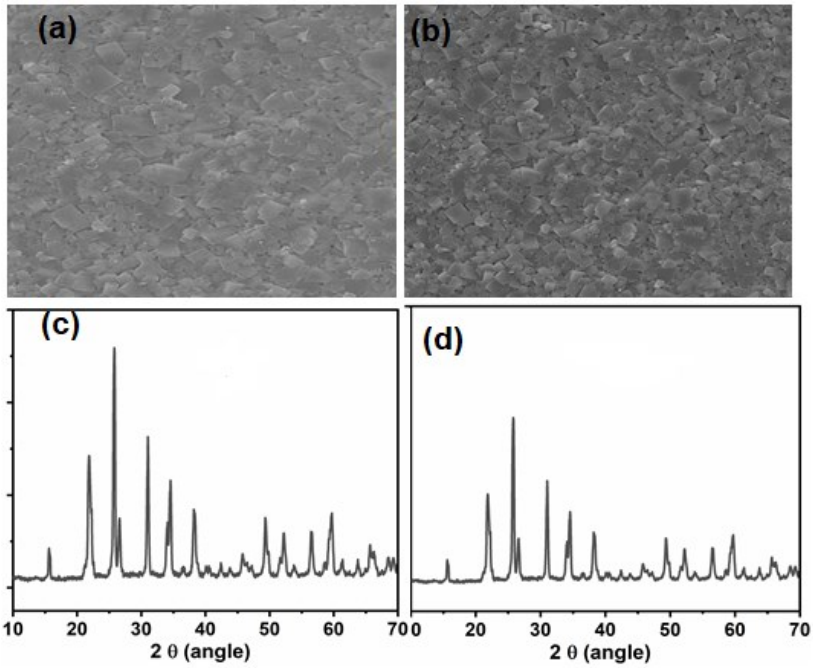

Figure S12: SEM images of LAMGP pellet (a) as synthesized (b) after soaking in LE for 10 days. XRD pattern of LAMGP pellet (c) as synthesized (d) after soaking in LE for 10 days.

Figure S13 displays the Raman spectra of the LAMGP pellet before and after soaking in LE. The spectra for LAMGP pellet before soaking in liquid electrolyte show many strong Raman bands, attributed to the vibrations of units in the material.[8] Similarly, no new peak was noticed

in the Raman spectroscopy measurement after soaking of the LAMGP pellet in the liquid electrolyte, which indicates that the LAMGP pellet is chemically stable towards the used LE. Moreover, the chemical compatibility between the LE and the LAMGP pellet was further examined using ICP-OES measurement over the LE, which have been used to soak the pellet. The ICP-OES measurement was employed to detect if Mg^{2+}, Al^{3+} and Ge^{4+} ions were remained in the LE when the LAMGP pellet soaked. From the ICP-OES measurement there was no Mg^{2+}, Al^{3+} or Ge^{4+} ion detected. This indicates there is no any chemical reaction between the LE and the pellet, a further confirmation good chemical compatibility between the LE and the LAMGP pellet.

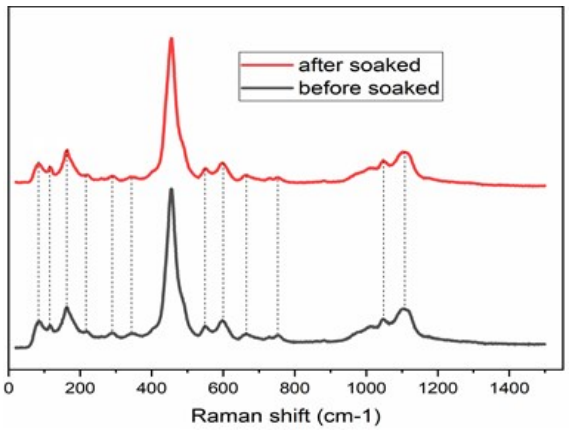

Figure S13: Comparison of Raman spectra of LAMGP pellets before and after being soaked in LE for 10 days.

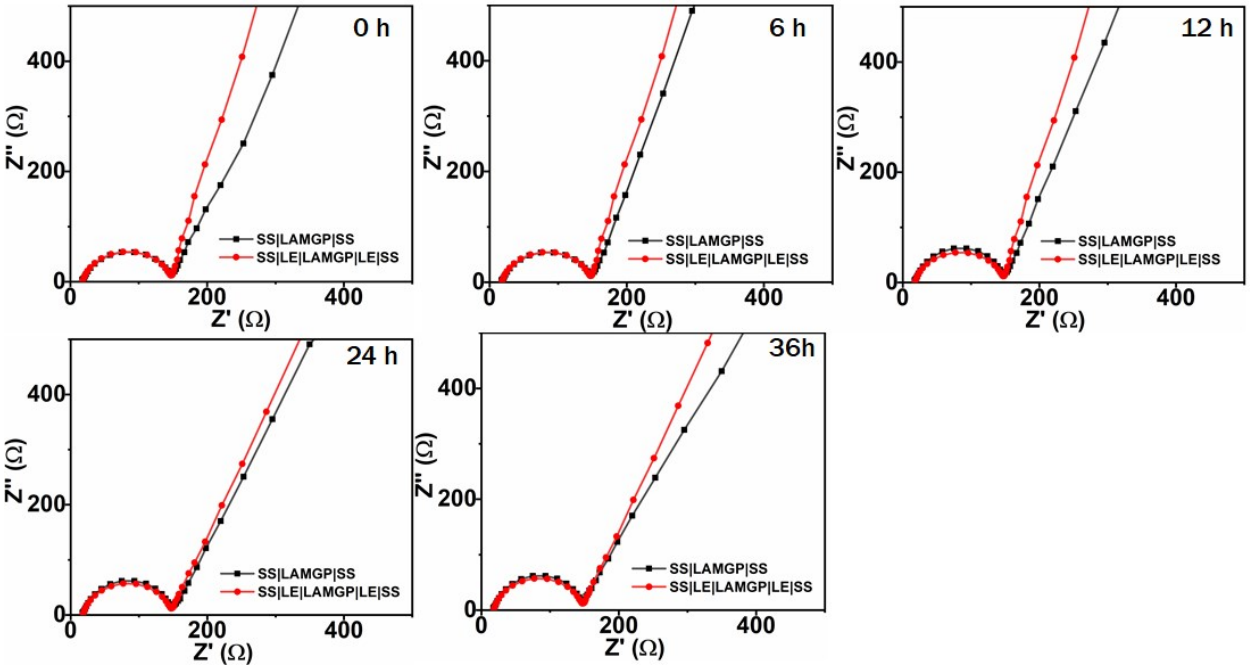

Figure S14: EIS results of SS|LAMGP|SS and SS|LE|LAMGP|LE|SS as function of time.

Table S10: summary of the electrochemical performance of cells with different configurations.

Electrolyte	Coulombic efficiency		Initial Capacity mA h g^{-1}		Capacity Retention
	1st cycle	average	charge capacity	discharge capacity	
LAMGP/10 μL LE	86.7%	98.14%	167.6	145.4	80.5% after 250 cycles
LAGP/10 μL LE	84.2%	97.89%	154.7	130.3	80.5% after 155 cycles
10 μL LE	91.6%		188.3	172.5	

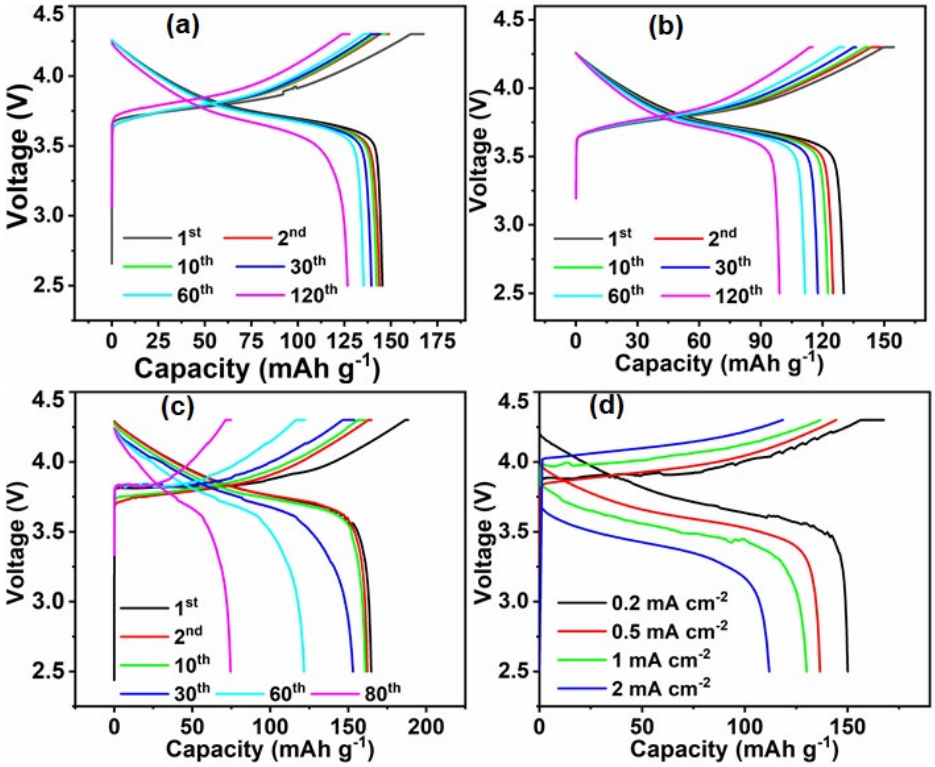

Figure S15: Charge/discharge profiles at different cycles of the cells at 0.2 mA cm^{-2} and 25 ^{o}C. (a). Li/LE/LAMGP/LE/NMC, (b).. Li/LE/LAGP/LE/NMC, (c) Li/10µL LE/NMC and (d). charge-discharge curves of Li/LE/LAMGP/LE/NMC cell at different current densities, varying from 0.2 mA cm^{-2} to 2 mA cm^{-2}.

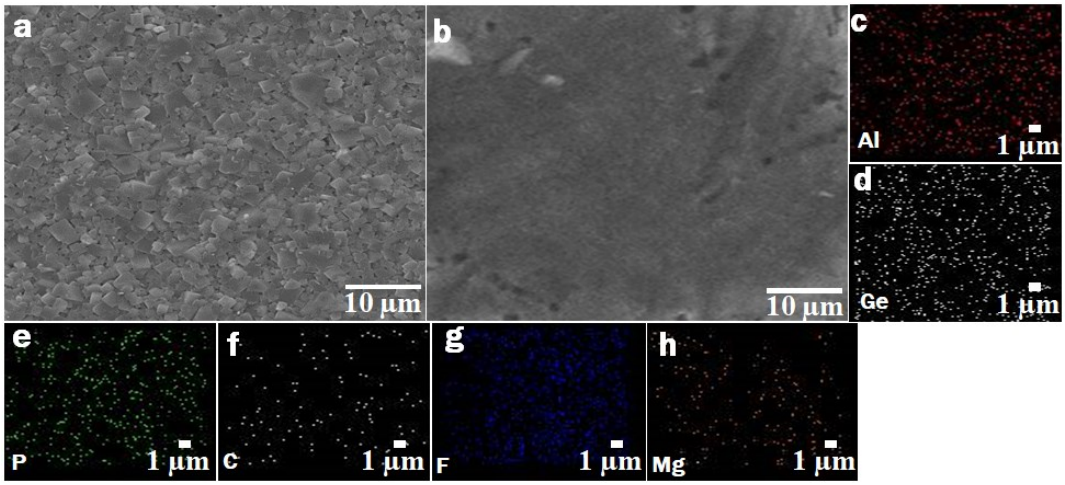

Figure S16. LAMGP pellet SEM images for post cycling SELEI analysis**.** (a). before cycling. (b). after 120 cycles. (c-g). after cycling EDS mapping of elements after 120 cycles.

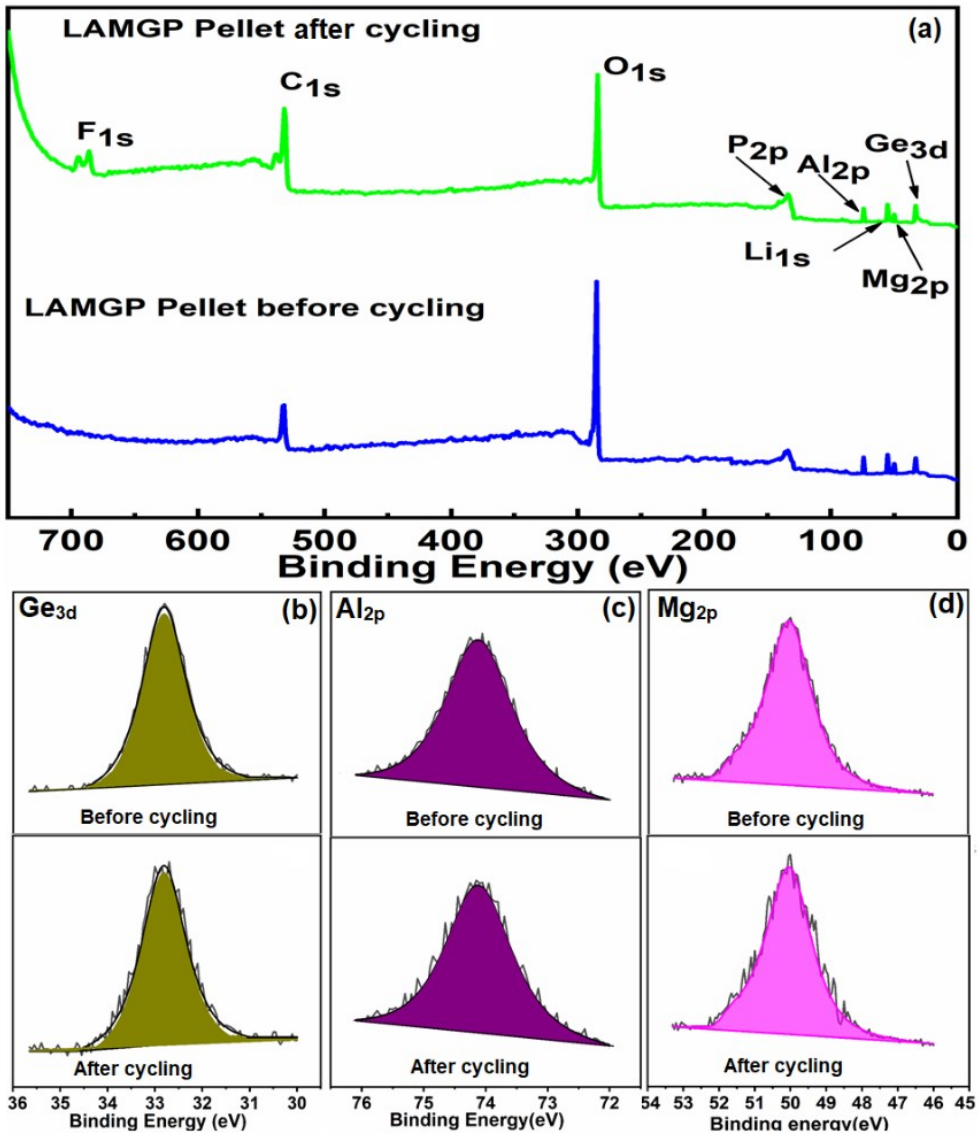

Figure S17: X-ray photoelectron spectra before and after electrochemical cycling (a). full survey of LAMGP pellets and (b-d). for Ge, Al and Mg, respectively.

References

1. T. Hou, G. Yang, N. N. Rajput, J. Self, S.-W. Park, J. Nanda and K. A. Persson, *Nano Energy*, 2019, **64**, 103881.

2. J. S. Thokchom and B. Kumar, *J. Power Sources*, 2010, **195**, 2870-2876.

3. M. Illbeigi, A. Fazlali, M. Kazazi and A. H. Mohammadi, *Solid State Ion.*, 2016, **289**, 180-187.

4. Y. Nikodimos, M.-C. Tsai, L. H. Abrha, H. H. Weldeyohannis, S.-F. Chiu, H. K. Bezabh, K. N. Shitaw, F. W. Fenta, S.-H. Wu, W.-N. Su, C.-C. Yang and B. J. Hwang, *J. mater. chem. A*, 2020, **8**, 11302-11313.

5. M. Kotobuki, E. Hanc, B. Yan, J. Molenda and L. Lu, *Ceram. Int.*, 2017, **43**, 12616-12622.

6. X. Xu, Z. Wen, X. Wu, X. Yang and Z. Gu, *J AM CERAM SOC*, 2007, **90**, 2802-2806.

7. J. S. Thokchom and B. Kumar, *J. Power Sources*, 2008, **185**, 480-485.

8. S. Pershina, A. Pankratov, E. Vovkotrub and B. Antonov, *Ionics*, 2019, **25**, 4713-4725.